

Alma Mater Studiorum Università di Bologna  
Archivio istituzionale della ricerca

Data-driven model predictive control of transcritical CO<sub>2</sub> systems for cabin thermal management in cooling mode

This is the final peer-reviewed author's accepted manuscript (postprint) of the following publication:

*Published Version:*

Wang H., Wang W., Song Y., Yang X., Valdiserri P., Rossi di Schio E., et al. (2023). Data-driven model predictive control of transcritical CO<sub>2</sub> systems for cabin thermal management in cooling mode. APPLIED THERMAL ENGINEERING, 235, 1-12 [10.1016/j.applthermaleng.2023.121337].

*Availability:*

This version is available at: <https://hdl.handle.net/11585/942735> since: 2024-01-26

*Published:*

DOI: <http://doi.org/10.1016/j.applthermaleng.2023.121337>

*Terms of use:*

Some rights reserved. The terms and conditions for the reuse of this version of the manuscript are specified in the publishing policy. For all terms of use and more information see the publisher's website.

This item was downloaded from IRIS Università di Bologna (<https://cris.unibo.it/>).  
When citing, please refer to the published version.

(Article begins on next page)

This is the final peer-reviewed accepted manuscript of:

Haidan Wang, Wenyi Wang, Yulong Song, Xu Yang, Paolo Valdiserri,  
Eugenia Rossi di Schio, Gangxu Yu, Feng Cao

Data-driven model predictive control of transcritical CO<sub>2</sub> systems  
for cabin thermal management in cooling mode

In: Applied Thermal Engineering, Volume 235, 2023

The final published version is available online at:

<https://doi.org/10.1016/j.applthermaleng.2023.121337>

Rights / License:

The terms and conditions for the reuse of this version of the manuscript are specified in the publishing policy. For all terms of use and more information see the publisher's website.

*This item was downloaded from IRIS Università di Bologna (<https://cris.unibo.it/>)*

***When citing, please refer to the published version.***

# **Data-driven model predictive control of transcritical CO<sub>2</sub> systems for cabin thermal management in cooling mode**

Haidan Wang<sup>a, b</sup>, Wenyi Wang<sup>a</sup>, Yulong Song<sup>a</sup>, Xu Yang<sup>a\*</sup>, Paolo Valdiserri<sup>b</sup>, Eugenia Rossi di Schio<sup>b</sup>, Gangxu Yu<sup>c</sup>, Feng Cao<sup>a\*</sup>

<sup>a</sup> School of Energy and Power Engineering, Xi'an Jiaotong University, Xi'an 710049, China

<sup>b</sup> Department of Industrial Engineering, University of Bologna, Bologna, Italy

<sup>c</sup> Yutong Bus Co., Ltd., Zhengzhou, China

\*Corresponding author, Email: [fcdo@mail.xjtu.edu.cn](mailto:fcdo@mail.xjtu.edu.cn) (Feng Cao); [yangzx@mail.xjtu.edu.cn](mailto:yangzx@mail.xjtu.edu.cn) (Xu Yang)

Tel: 86-029-82663583;

Fax: 86-029-82663583

## **Abstract**

The transcritical CO<sub>2</sub> cabin thermal management system has gained significant attention in the field of electric vehicles due to its outstanding heating performance and environmental advantages. However, ensuring its optimal operation in real-time during vehicle operation poses a challenge. Amongst these challenges, controlling the optimal discharge pressure is particularly difficult. In this paper, we propose a novel model predictive controller that focuses on the cabin cooling mode. The controller utilizes a high-fidelity data-driven dynamic model of the transcritical CO<sub>2</sub> system, coupled with a dynamic thermal model of the cabin. By simultaneously controlling the compressor, electronic expansion valve, and indoor fan, the proposed controller enables the cabin thermal management system to operate in real-time at the optimal discharge pressure while ensuring passenger comfort, thereby minimizing the total power consumption of the system. Additionally, two model predictive control strategies, focused on comfort and energy-saving, respectively, are introduced. Through simulations under various conditions over a 6-hour period, comparing the PI controller, the comfort priority model predictive controller reduces energy consumption by 13.33%, and the energy-saving priority model predictive controller achieves a 20.27% reduction. The proposed novel model predictive controller exhibits energy-saving advantages.

# 1 Keywords

- 2 Transcritical CO<sub>2</sub> system, Air conditioning system, Model predictive control, Dynamic  
3 thermal model, Energy conservation.

## Nomenclature

A	Area, (m <sup>2</sup> )	$V_{disp}$	Displacement, (m <sup>3</sup> )
AC	Air conditioning	<b>Greek symbols</b>	
CLTC	China Automotive Test Cycle		
COP	Coefficient of performance	$\alpha$	Surface heat transfer coefficient, (W/(m <sup>2</sup> ·K))
$c_p$	Specific heat capacity, (J/(kg·K))	$\xi$	Pressure ratio of compressor
EEV	Electronic expansion valve	$\eta_e$	Compressor motor efficiency
EV	Electric vehicle	$\eta_{is}$	Compressor isentropic efficiency
ESC	Extreme seeking control	$\eta_V$	The ratio of the theoretical volume of the expander to the compressor
HFC	Hydrofluorocarbon	$\rho$	Density, (kg/m <sup>3</sup> )
GA	Genetic algorithm	$\tau$	Time, (s)
GWP	Global warming potential	<b>Subscripts</b>	
h	Enthalpy, (J/kg)		
HP	Heat pump	a	Ambient
IHX	Internal heat exchanger	air	Air
$I_{solar}$	Intensity of solar radiation, (W/m <sup>2</sup> )	cabin	Cabin
MPC	Model predictive controller	cl	Clothes
M	Metabolic rate of the passenger, (W/m <sup>2</sup> )	com	Compressor
m	Mass, (kg)	dis	Discharge of Compressor
$\dot{m}$	Mass flow rate, (kg/s)	evap	Evaporator
N <sub>com</sub>	Speed of compressor, (RPM)	EEV	Electronic expansion valve
P	Pressure, (bar)	fan	Indoor fan
PMV	Predicted Mean Vote	hp	High pressure
$\dot{Q}$	Quantity of heat, (W)	in	Inlet
$R_{cl}$	clothes thermal resistance of the passenger, (m <sup>2</sup> ·°C/W)	lp	Low pressure
rH	Relative humidity	out	Outdoor
T	Temperature, (°C)	send	Out let air of evaporator
TCCTMS	Transcritical CO <sub>2</sub> cabin thermal management system	suc	Suction of the compressor
$\dot{v}_{car}$	Vehicle speed, (m/s)		

## 1. Introduction

The thermal management systems of electric vehicles (EVs) have raised numerous concerns regarding energy conservation and environmental protection [1]. Hydrofluorocarbons (HFCs) refrigerants, with R134a being a representative example, are widely used as working fluids. However, they have high global warming potential (GWP) values, which necessitates their gradual replacement [2]. Furthermore, due to their low evaporating pressure and low suction density, heat pump systems with HFCs have limited heating capacity and high-power consumption in colder winter conditions, exacerbating range anxiety for electric vehicles during winter seasons. However, as a natural refrigerant, CO<sub>2</sub> has gained more attention from an environmental protection standpoint. And transcritical CO<sub>2</sub> heat pump (HP) systems provide significant benefits in terms of heating performance, particularly under low-temperature heating circumstances [3-6]. Transcritical CO<sub>2</sub> systems thus have a tremendous deal of potential to develop into the most effective thermal management systems for electric vehicles.

Due to the characteristics of supercritical CO<sub>2</sub> fluid, experiments and theoretical research have shown that the discharge pressure in the transcritical CO<sub>2</sub> system must be optimized in order to maximize the coefficient of performance (COP) [7-8]. The system power consumption will be significantly decreased at the optimal discharge pressure. Therefore, the control strategy is very important for the transcritical CO<sub>2</sub> cabin thermal management system (TCCTMS).

Model predictive controllers (MPC) with flexible control framework, automatic optimization capabilities, and strong robustness are more suitable for thermal management systems [9]. Many scholars have applied MPC technology to subcritical refrigeration systems represented by R134a. Xie et al. [10-11] established models for the R134a AC and HP systems. They proposed the selection of state variables and designed an MPC predictive controller to control the compressor and fan speeds, while the control of the throttle valve still adopted PID control. Moreover, Glos et al. [12] proposed a MPC scheme for cabin temperature and air quality control, which is applicable for vehicle standstill conditions, assuming that the COP values are constant. A stochastic MPC is proposed by He et al. [13] to enhance the energy efficiency of the

AC systems, they established a thermal load model and employed a topological graph to search for the value of COP. Schaut and Sawodny [14] proposed and validated an optimization-based TCCTMS that minimized energy consumption and maximized thermal comfort. MPC combined with different forecast methods of passenger number was prepared in [15-16] for cabin temperature control of an electric bus. In their modeling of the AC system, they introduced the compressor volumetric efficiency and suction gas density to determine the compressor's speed. Hemmati [17] et al. developed fast and efficient thermal dynamics models of vehicle cabin, powertrain, and exhaust aftertreatment system for a test vehicle, and used them for multi-objective optimization of vehicle operation. For the thermal management system, the scholars developed more detailed thermal models for both the battery and the cabin. Regarding the COP, they considered using fixed values or empirical formulas. A hierarchical MPC strategy is developed by Zhang and Tong [18] for the cooperative control of vehicle speed and cabin temperature. Xie et al. [19] developed an MPC for the battery thermal management system, considering both energy saving and battery lifespan. In a similar vein, Liu et al. [20] proposed a self-adaptive intelligent neural network-based MPC specifically designed for an air-based battery thermal management system; Park et al. [21] introduced a stochastic algorithm to the MPC strategy. MPC schemes were also proposed for combined cabin and battery thermal management in [22]. Guo et al. [23], Gong et al. [24] and Guo et al. [25] demonstrated the energy-saving superiority of MPC controllers applied to hybrid electric vehicles.

However, the control of CO<sub>2</sub> transcritical systems is more complex than that of HFC refrigerant systems, such as R134a, because the expansion valve in HFC systems is usually used to regulate the evaporator outlet superheat to a constant value, while the CO<sub>2</sub> system needs to adjust the expansion valve to achieve the optimal discharge pressure. Moreover, it is very laborious to establish the topology map and correlation of the optimal COP of the transcritical CO<sub>2</sub> system under various operating conditions. For the optimal control of the transcritical CO<sub>2</sub> system, some scholars fit a variety of empirical correlations and various intelligent algorithms to characterize the optimal discharge pressure in order to determine the PID controller's control goals [26-36].

1 However, the empirical formulae, demand a lot of experimental data and artificially  
2 seek the optimal value, and these PID-based controllers are all feedback control  
3 schemes and often introduce a little delay. In addition, extreme seeking control (ESC)  
4 has been widely concerned because of its optimization function [37-40]. But the  
5 convergence time problem prevents ESC from being used in situations when the  
6 disturbance is rapidly fluctuating, especially for automotive air-conditioning systems.  
7 Besides, it is difficult to increase the output variables of ESC to more than 2 for the  
8 optimization process. Researchers have started to introduce MPC control methods into  
9 the control of transcritical CO<sub>2</sub> systems. Wang et al. [41] applied a data-driven MPC to  
10 the transcritical CO<sub>2</sub> heat pump water heater and realized the control of the throttle  
11 valve area and water flow. However, it does not consider the adjustment of compressor  
12 speed, which is a very important control target. Zhang et al. [42] used MPC to control  
13 the compressor speed and indoor fan speed in the transcritical CO<sub>2</sub> system of the  
14 railway air conditioning, but this MPC does not have the function of finding the optimal  
15 discharge pressure.

16 It can be seen from previous studies that MPC is an advanced algorithm to solve  
17 the control problem of cabin/battery thermal management system. However, for  
18 transcritical CO<sub>2</sub> systems, it is very difficult to establish an empirical formula or a  
19 topology map of the optimal COP that covers all operating conditions. And as far as we  
20 know, no scholar has proposed the model predictive control method to realize  
21 simultaneous control of the compressor, fan and throttle valve in TCCTMS. This study  
22 proposes a data-driven nonlinear MPC that has the following features: (1) It can operate  
23 the compressor, throttle valve, and indoor fan to meet passengers comfort requirements  
24 while saving power consumption; (2) It does not need an additional PI controller, nor  
25 does it require extensive experiments to manually search for the optimal discharge  
26 pressure; (3) It accurately considers the dynamic COP of the transcritical CO<sub>2</sub> system  
27 in cabin cooling mode. In addition, to compare the control effect of MPC, we installed  
28 the traditional feedback controllers-On/Off-PI controller and PI controller-in the same  
29 system. The data-driven model can be updated according to the changes in the system  
30 to avoid the inaccurate optimization problem caused by the performance changes of

system components.

## 2. System description and modeling details

### 2.1 Simulation model

In Fig. 1, a schematic representation of a typical transcritical CO<sub>2</sub> AC system is displayed. In addition to the compressor, evaporator, gas-cooler, and electronic expansion valve (EEV) used in the refrigeration system, internal heat exchangers (IHX) and accumulators are parts of the transcritical CO<sub>2</sub> system. IHX is used to lower the gas-cooler's outlet temperature in order to increase COP. Additionally, using an accumulator can prevent the liquid CO<sub>2</sub> from being sucked into the compressor under a number of operational conditions.

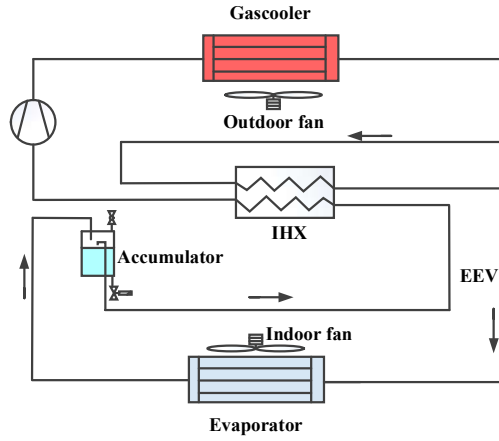


Fig. 1 schematic representation of a typical transcritical CO<sub>2</sub> AC system.

The current research uses GT-Suite, a tool that is often used in the analysis of thermal management systems for EVs, in order to build the simulation models for the transcritical CO<sub>2</sub> AC systems. Table 1 displays the modeling specifics of each component. Table 2 presents the component parameters of the AC system designed by the authors.

Table 1

The modeling specifics of components.

Equipment name	Modules in GT	Specification
Compressor	<i>CompPosDispRefrig</i> and <i>SpeedBoundaryRot</i>	$\dot{m}_{CO_2} = V_{disp} \cdot \eta_v \cdot N_{com} \cdot \rho_{suc}$ $\dot{W}_{com} = \dot{m}_{CO_2} \cdot \frac{h_{dis} - h_s}{\eta_{is}} \cdot \frac{1}{\eta_e}$



		$\eta_{is} = f(N_{com}, \xi, T_{suc})$ $\eta_v = f(N_{com}, \xi, T_{suc})$ $\eta_e = f(\xi)$ $\dot{Q}_{HX} = \dot{m}_{CO_2}(h_{CO_2,out} - h_{CO_2,in}) = \dot{m}_{air}c_{p,air}(T_{air,out} - T_{air,in})$
Evaporator and Gascooler	<i>HxMaster</i> and <i>HxSlave</i>	$\dot{Q}_{HX} = \sum_{j=1}^N \alpha_j A_{i,j} (T_{CO_2,j} - T_{air,j})$ $\alpha_j = \left( \frac{1}{\alpha_{CO_2,j}} + \frac{A_{in,j}}{\alpha_{air,j} A_{out,j}} \right)^{-1}$ $\dot{Q}_{HX} = \dot{m}_{CO_2}(h_{CO_2,hp,out} - h_{CO_2,hp,in}) = \dot{m}_{CO_2}(h_{CO_2,lp,out} - h_{CO_2,lp,in})$ $\dot{Q}_{HX} = \sum_{j=1}^N \alpha_j A_{i,j} (T_{CO_2,hp,j} - T_{CO_2,lp,j})$ $\alpha_j = \left( \frac{1}{\alpha_{CO_2,hp,j}} + \frac{1}{\alpha_{CO_2,lp,j}} \right)^{-1}$
EEV	<i>OrificeConn</i>	$\dot{m}_{CO_2} = C_q \cdot A_{EEV} \cdot \sqrt{\frac{2\Delta P \cdot \rho_{EEV,in}}{k_{dp}}}$
Accumulator	<i>AccumulatorRefrig</i>	
Indoor Fan	<i>FanFlow</i>	$\dot{W}_{fan} = f(\dot{m}_{air})$

- 1
- 2 Table 2
- 3 The parameters of the components for the designed transcritical CO<sub>2</sub> AC system.

Equipment name	Specification
Compressor	Displacement: 8.2 cm <sup>3</sup> Speed range: 1000~8000 RPM
Evaporator	Type: Micro-channel fin-tube; Dimension: 230 mm (length), 230 mm (height), 32 mm (width)
Gascooler	Type: Micro-channel fin-tube; Dimension: 660 mm (length), 515 mm (height), 16 mm (width)
Internal Heat Exchanger	Type: concentric tube heat exchanger; Length: 1600 mm; Outer pipe diameter: 22 mm, Inner pipe diameter: 16 mm

Accumulator

1.1 L

Indoor Fan

0~0.18 kg/s

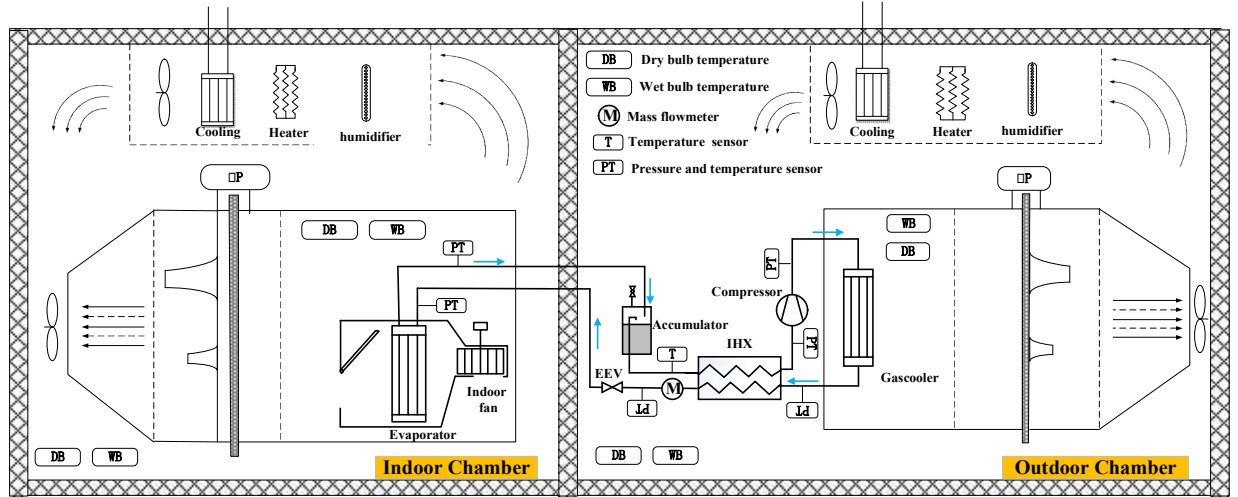
The compressor isentropic efficiency  $\eta_{is}$ , volumetric efficiency  $\eta_v$  and motor efficiency  $\eta_e$  are determined by compressor speed ( $N_{com}$ ), pressure ratio ( $\xi$ ), and suction temperature ( $T_{suc}$ ). The power consumption of the indoor fan is determined by the mass flow of air ( $\dot{m}_{air}$ ). The correlations are fitted from the experimental data.

## 2.2 Experimental verification of the transcritical CO<sub>2</sub> system

Two separate enthalpy difference chambers were used for a series of experimental tests on the transcritical CO<sub>2</sub> system's test rig. Fig.2 depicts the photo of the test rig and the configuration of the enthalpy difference chamber. The principles of the experimental setup and the specific parameters of its components have been described in detail in Section 2.1. The surrounding environment's temperature and humidity may be separately controlled by each enthalpy difference chamber. During the experiment, the temperature of the outdoor chamber was set at 30 °C ~ 40 °C, and the compressor speed varied from 1000 RPM to 4000 RPM. Under these test conditions, the power consumption and cooling capacity were assessed. Table 3 displays the parameters experimental measurement devices and uncertainties.



(a) Photo of the test rig.



(b) Configuration of the enthalpy difference chamber.  
Fig.2 The photo and the schematic diagram of the test rig.

Table 3

The parameters experimental measurement devices, and uncertainties.

Parameter	Component	Range and uncertainties
Air wet/dry bulb temperature	PT100 thermoelectrical resistance	-50~200 °C, $\pm (0.15 + 0.0002 \times \text{reading})$ °C
CO <sub>2</sub> fluid temperature	K-type thermocouple	-50~200 °C, $\pm 0.5$ °C
Pressure	MPM489 transmitter	0~20 MPa, 2.5 % of the range
Power	WT500	15~1000 V and 0.5~40 A, $\pm 0.1\%$ of reading + 0.1% of the range.
Mass flow rate	Micro Motion Mass flowmeter	11500 kg·h <sup>-1</sup> , $\pm 1\%$

The error propagation for the cooling capacity and COP was calculated using the Kline and McClintock [43] method. The largest uncertainty of the cooling capacity and COP (the cooling capacity divided by the compressor power consumption) were 3.83% and 3.85%, respectively. Fig. 3 shows that all the data deviation ranges for power consumption and cooling capacity are within 5%, demonstrating the viability of the simulation model.

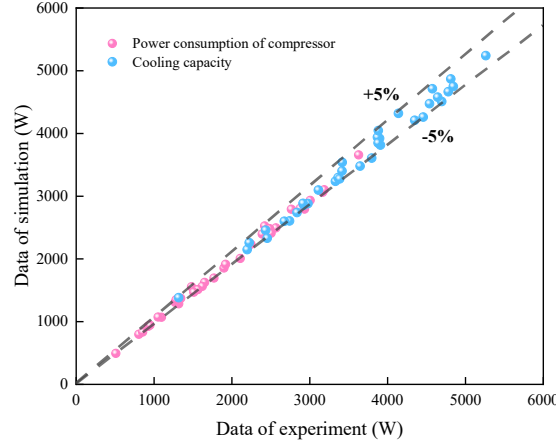


Fig.3 Experimental verification of physical model.

### 3. Model predictive controller for TCCTMS

#### 3.1 Dynamic thermal model of Cabin

The surrounding environment, the speed of the vehicle, and the cooling capabilities of AC system all affect the temperature within the cabin of the EV. The variation in cabin temperature can be written as follows:

$$\frac{dT_{cabin}}{d\tau} = \frac{\dot{Q}_{cabin}}{m_{air} * c_{p,air}} \quad (1)$$

$\dot{Q}_{cabin}$  is made up of a number of loads, including heat input from solar radiation ( $\dot{Q}_{rad}$ ), convective heat moving between the interior air and the cabin surfaces ( $\dot{Q}_{con}$ ), load from passengers ( $\dot{Q}_{people}$ ) and electronic equipment ( $\dot{Q}_W$ ), heat load from ventilation and air leakage ( $\dot{Q}_{air}$ ), and heat removed by the air conditioning system ( $\dot{Q}_{AC}$ ).

$$\dot{Q}_{cabin} = \dot{Q}_{rad} + \dot{Q}_{con} + \dot{Q}_{people} + \dot{Q}_W + \dot{Q}_{air} - \dot{Q}_{AC} \quad (2)$$

The heat input load from solar radiation is

$$\dot{Q}_{rad} = \varepsilon_t * I_{solar} * A_{glass} \quad (3)$$

where  $A_{glass}$  is the area of the glass,  $m^2$ ;  $\varepsilon_t$  is the transmission factor;  $I_{solar}$  is the intensity of solar radiation,  $W/m^2$ .

$\dot{Q}_{con}$  is the thermal convection between the cabin air and the glass, the roof, the body side and the floor,

$$\dot{Q}_{con} = \sum_i A_i * \alpha_{in} * (T_i - T_{cabin}) \quad (4)$$

where  $T_i$  and  $A_i$  are the average temperature and total area of the four parts,  $^{\circ}C$  and

m<sup>2</sup>, respectively.

The temperature variation of these parts can be written as follows:

$$\frac{dT_i}{d\tau} = \frac{\dot{Q}_{abs,i} + \dot{Q}_{r,i} - \dot{Q}_{con,in,i} - \dot{Q}_{con,out,i}}{m_i * c_{p,i}} \quad (5)$$

$$\dot{Q}_{abs} = \varepsilon_a * I_{solar} * A_i \quad (6)$$

$$\dot{Q}_r = \sigma * \varepsilon_e * A_i * (T_a^4 - T_i^4) \quad (7)$$

$$\dot{Q}_{con,in} = A_i * \alpha_{in} * (T_i - T_{cabin}) \quad (8)$$

$$\dot{Q}_{con,out} = A_i * \alpha_{out} * (T_i - T_a) \quad (9)$$

where  $\varepsilon_a$  and  $\varepsilon_e$  are the absorption factor and equivalent emission factor;  $\alpha_{in}$  is the convective heat transfer coefficient between cabin surface and cabin air, W/(m<sup>2</sup>·K);  $\alpha_{out}$  is the convective heat transfer coefficient between the cabin surface and ambient, which mainly depends on the speed of the vehicle, W/(m<sup>2</sup>·K). The  $\dot{Q}_{people}$ ,  $\dot{Q}_W$  and  $\dot{Q}_{air}$  are considered constants [10].

The heat removed by the AC system can be calculated as,

$$\dot{Q}_{AC} = \dot{m}_{air} * c_{p,air} * (T_{cabin} - T_{send}) \quad (10)$$

where  $T_{send}$  represents the temperature of the cold air sent into the cabin by the indoor fan, °C;  $\dot{m}_{air}$  is the air mass flow passing through the evaporator, kg/s.

### 3.2 Nonlinear transcritical CO<sub>2</sub> system identification

This work employs a data-driven nonlinear state-space model to depict the transcritical CO<sub>2</sub> system owing to its high level of nonlinearity. The nonlinear model builds on a range of nonlinear candidate functions to identify the original system from the simulation data. The transcritical CO<sub>2</sub> system can be described by,

$$\mathbf{x}(k) = f(\mathbf{x}(k-1), \mathbf{u}(k-1), \mathbf{d}(k-1)) \quad (11a)$$

$$\mathbf{y}(k) = g(\mathbf{x}(k), \mathbf{u}(k), \mathbf{d}(k)) \quad (11b)$$

where  $\mathbf{x}$ ,  $\mathbf{u}$ ,  $\mathbf{d}$  and  $\mathbf{y}$  represent system state vector, inputs vector, disturbance vector, and output vector.

For the transcritical CO<sub>2</sub> system, it is possible to control the cooling capacity and COP by modifying the  $N_{com}$  and the flow area of EEV ( $A_{EEV}$ ).  $T_{send}$  accurately

measures the system's cooling capacity when both the evaporator inlet air temperature ( $T_{cabin}$  in this paper) and  $\dot{m}_{air}$  are constant. Meanwhile, the most significant variables influencing the system COP are  $P_{dis}$ ,  $P_{evap}$ , and  $T_{EEVin}$ . As external disturbances to the transcritical CO<sub>2</sub> system, the  $\dot{m}_{air}$ , the  $T_{cabin}$ , and the ambient temperature  $T_a$  are all taken into consideration.

$$\mathbf{x} = [T_{send} \ P_{dis} \ P_{evap} \ T_{EEVin}]^T \quad (12a)$$

$$\mathbf{u} = [N_{com} \ A_{EEV}]^T \quad (12b)$$

$$\mathbf{d} = [\dot{m}_{air} \ T_{cabin} \ T_a]^T \quad (12c)$$

$$\mathbf{y} = [\dot{W} \ COP]^T \quad (12d)$$

where,

$$\dot{W} = \dot{W}_{com} + \dot{W}_{fan} \quad (12e)$$

$$COP = \frac{\dot{Q}_c}{\dot{W}} \quad (12f)$$

Genetic Algorithm (GA) may be attributed as a method for optimizing the search tool for difficult problems based on the genetics selection principle [44]. The advantage of the GA algorithm is model-free. Here, the model-free means that we can skip the process of the design of the numerical model and pre-selected parameters. For example, the ref. [10] shows a flowchart of a complex process of design and pre-selected parameters. However, in this strategy, we introduce a simple numerical model but obtain a promising result (i.e., reach above 95% accuracy). The comparison results show that the GA algorithm has an advantage in model design.

Fig.4 shows the workflow of searching for the optimal control-oriented model of the transcritical CO<sub>2</sub> system using the GA. The  $\beta$ , coefficients for the linear combination, required to be estimated for nonlinear system identification. The first step in determining the best nonlinear model is to pick the initial population and evaluate the fitness factor of each chromosome to select the next-generation parent. The coefficient of determination, R-square, has been selected to determine the optimal  $\beta$ ,

$$R - square = \frac{SSR}{SST} \quad (13a)$$

Sum of squares of the regression,

$$SSR = \sum_{i=1}^n w_i * (\hat{y}_i - \bar{y}_i)^2 \quad (13b)$$

The total sum of squares,

$$SST = \sum_{i=1}^n w_i * (y_i - \bar{y}_i)^2 \quad (13c)$$

Where  $y_i$  is the real system output value;  $\bar{y}_i$  is the average of  $y_i$ ;  $\hat{y}_i$  presents the estimated system output value.

Crossover is the second step, which produces new offspring. After the crossover operation, mutation takes place to prevent all population solutions from settling into a local optimum of the solved issue. Up until the ideal nonlinear model is discovered, these procedures are repeated.

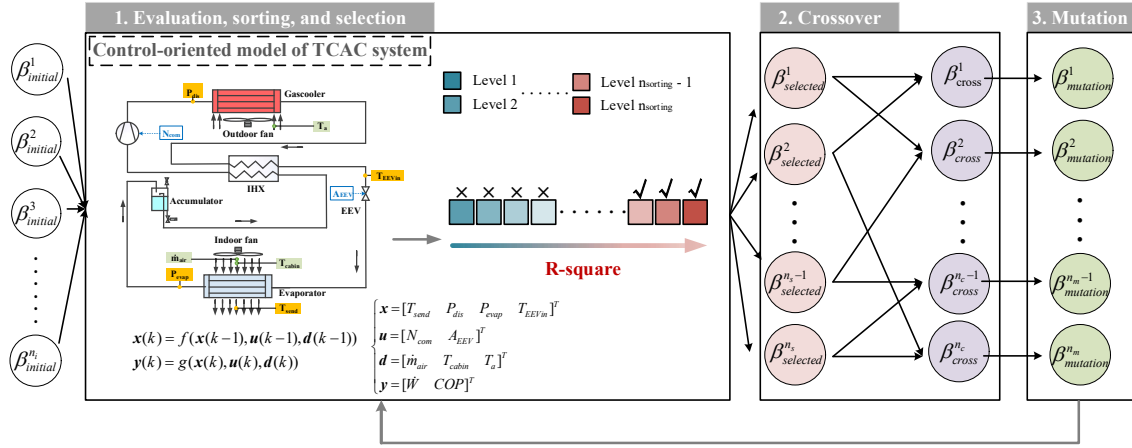


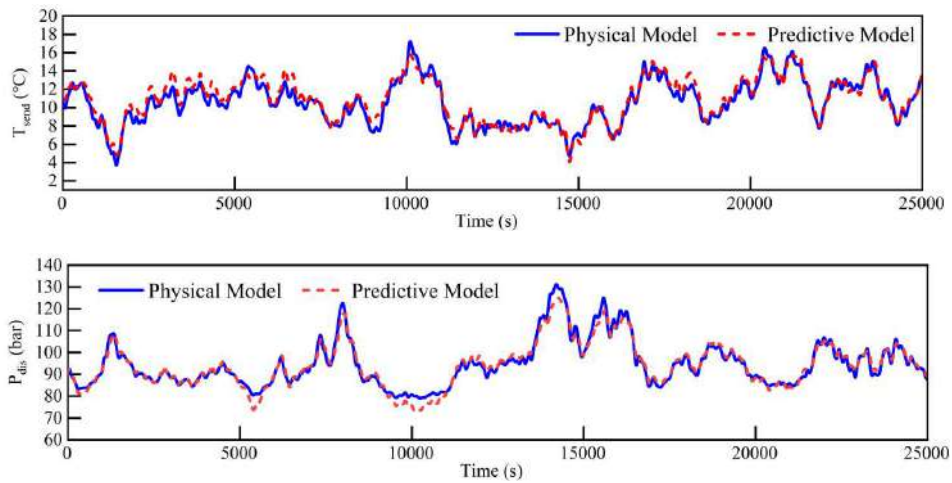
Fig.4 Workflow of searching for the optimal control-oriented model of the transcritical CO<sub>2</sub> system using the GA.

The Physical model verified by the experiment in Fig. 2 is used to produce the training and validation data. To represent a wide spectrum of system nonlinear dynamics, various operations are simulated under varying ambient temperatures, indoor fan air flow rates and cabin temperatures. The finalized data-driven model is:

$$\begin{bmatrix} T_{send,k+1} \\ P_{dis,k+1} \\ P_{evap,k+1} \\ T_{EEVin,k+1} \end{bmatrix} = \beta_{1,1}^T \begin{bmatrix} T_{send,k} \\ P_{dis,k} \\ P_{evap,k} \\ T_{EEVin,k} \end{bmatrix} + \beta_{1,2}^T \begin{bmatrix} N_{com,k} \\ A_{EEV,k} \end{bmatrix} + \beta_{1,3}^T \begin{bmatrix} \dot{m}_{air,k} \\ T_{cabin,k} \\ T_{a,k} \end{bmatrix} + \beta_{1,4}^T \quad (14a)$$

$$\begin{aligned}
1 \quad & \begin{bmatrix} \dot{W}_{com,k} \\ COP_k \end{bmatrix} = \beta_{2,1}^T \begin{bmatrix} T_{send,k} \\ P_{dis,k} \\ P_{evap,k} \\ T_{EEVin,k} \\ N_{com,k} \\ A_{EEV,k} \\ \dot{m}_{air,k} \\ T_{a,k} \\ T_{cabin,k} \\ 1 \end{bmatrix} \cdot T_{send,k} + \beta_{2,2}^T \begin{bmatrix} P_{dis,k} \\ P_{evap,k} \\ T_{EEVin,k} \\ N_{com,k} \\ A_{EEV,k} \\ \dot{m}_{air,k} \\ T_{a,k} \\ T_{cabin,k} \\ 1 \end{bmatrix} \cdot P_{dis,k} + \beta_{2,3}^T \begin{bmatrix} P_{evap,k} \\ T_{EEVin,k} \\ N_{com,k} \\ A_{EEV,k} \\ \dot{m}_{air,k} \\ T_{a,k} \\ T_{cabin,k} \\ 1 \end{bmatrix} \cdot P_{evap,k} + \\
2 \quad & \beta_{2,4}^T \begin{bmatrix} T_{EEVin,k} \\ N_{com,k} \\ A_{EEV,k} \\ \dot{m}_{air,k} \\ T_{a,k} \\ T_{cabin,k} \\ 1 \end{bmatrix} \cdot T_{EEVin,k} + \beta_{2,5}^T \begin{bmatrix} N_{com,k} \\ A_{EEV,k} \\ \dot{m}_{air,k} \\ T_{a,k} \\ T_{cabin,k} \\ 1 \end{bmatrix} \cdot N_{com,k} + \beta_{2,6}^T \begin{bmatrix} A_{EEV,k} \\ \dot{m}_{air,k} \\ T_{a,k} \\ T_{cabin,k} \\ 1 \end{bmatrix} \cdot A_{EEV,k} + \beta_{2,7}^T \begin{bmatrix} \dot{m}_{air,k} \\ T_{a,k} \\ T_{cabin,k} \\ 1 \end{bmatrix} \cdot \dot{m}_{air,k} + \\
3 \quad & \beta_{2,8}^T \begin{bmatrix} T_{a,k} \\ T_{cabin,k} \\ 1 \end{bmatrix} \cdot T_{a,k} + \beta_{2,9}^T \begin{bmatrix} T_{cabin,k} \\ 1 \end{bmatrix} \cdot T_{cabin,k} + \beta_{2,10}^T \quad (14b)
\end{aligned}$$

Fig.5 shows the validation of the finalized data-driven model. The physical model's running outcomes in GT-Suite are shown by the blue solid line, while the red dashed line shows the outputs predicted by the data-driven model using the same inputs and disturbance. The relative errors for  $T_{send}$ ,  $P_{dis}$ ,  $P_{evap}$ ,  $T_{EEVin}$ ,  $\dot{W}_{com}$ , and COP are 94.17%, 97.94%, 98.40%, 98.62%, 99.22%, and 96.26%, respectively. It is evident that the properties of the transcritical CO<sub>2</sub> system can be adequately described by the control-oriented model.





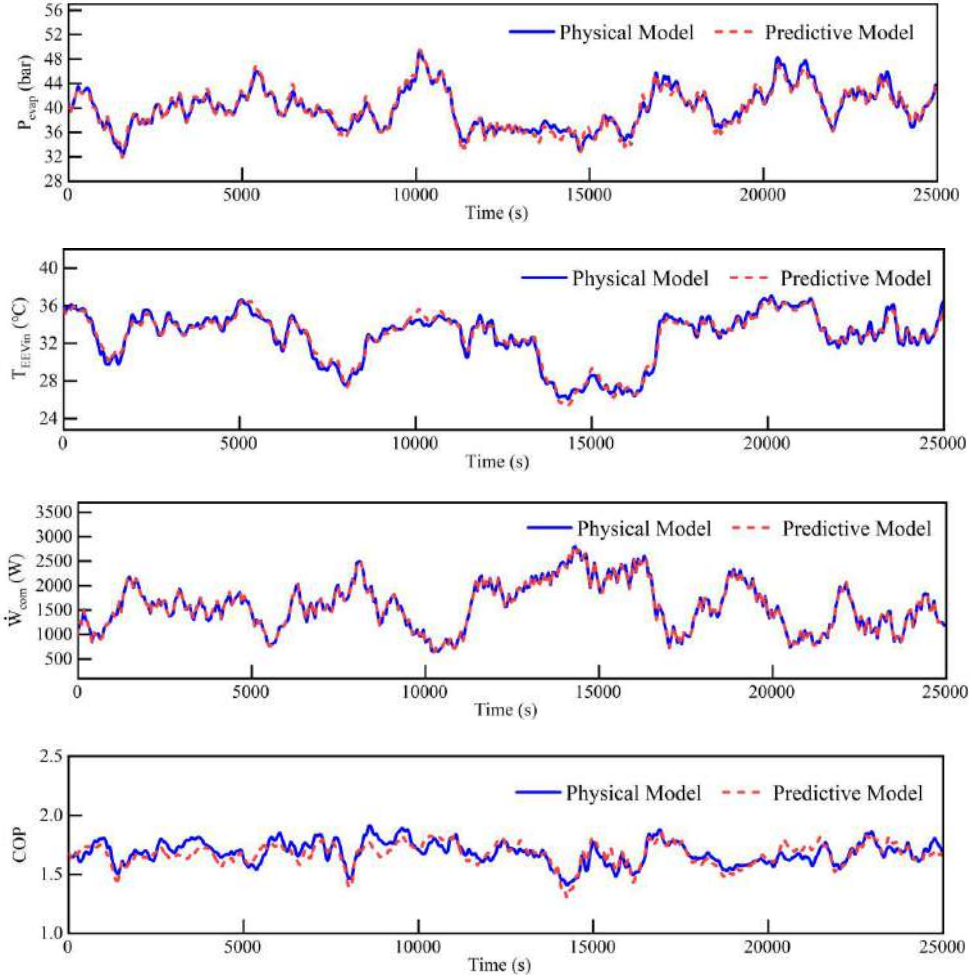


Fig.5 The validation of the model.

### 3.3 MPC controller for TCCTMS

Fig. 6 shows the TCCTMS controlled by the MPC. The system states are represented by the vector  $\mathbf{x}=[T_{\text{send}} \ P_{\text{dis}} \ P_{\text{evap}} \ T_{\text{EEVIn}} \ T_{\text{cabin}}]^T$ , and the control inputs are denoted by  $\mathbf{u}=[\dot{m}_{\text{air}} \ N_{\text{com}} \ A_{\text{EEV}}]^T$ . The system outputs are total power consumption and COP,  $\mathbf{y}=[\dot{W} \ \text{COP}]^T$ . The disturbance vector is given by  $\mathbf{d}=[I_{\text{rad}} \ \dot{v}_{\text{car}} \ T_{\text{a}}]^T$ .

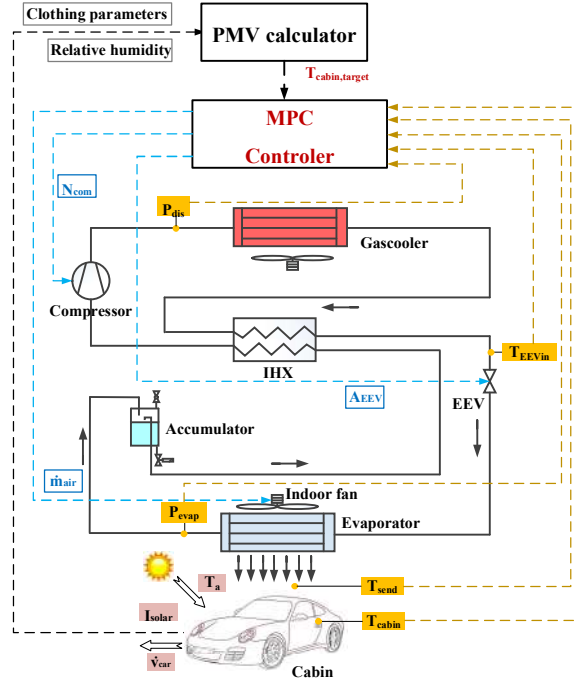


Fig.6 TCCTMS with MPC controller

The main objective of the data-driven MPC is to maximize system COP while maintaining the target cabin temperature:

$$\min_u J = r_1 \sum_{i=1}^N \left( T_{cabin}(k+i|k) - T_{cabin,target}(k+i|k) \right)^2 + r_2 \sum_{i=0}^N -COP(k+i|k) \quad (15a)$$

$$s. t. \begin{cases} x_{min} \leq x(k+i|k) \leq x_{max} & \forall i \leq N \\ u_{min} \leq u(k+i|k) \leq u_{max} & \forall i \leq N \\ \Delta u_{min} \leq \Delta u(k+i|k) \leq \Delta u_{max} & \forall i \leq N \end{cases} \quad (15b)$$

where  $N$  is the preceding horizon, selected as 4;  $r_1$  and  $r_2$  represent the weight coefficients of the two objectives respectively, selected as 10 and 0.1; The state vector at the time  $k+i$  predicted at the moment  $k$  is denoted by  $k+i|k$ . State vector  $x(k+j|k)$ , input vector  $u(k+j|k)$ , and the variation of input vector  $\Delta u(k+j|k)$  are limited by (15b).

In addition, the  $T_{cabin,target}$  is calculated by the Predicted Mean Vote (PMV) calculator, which can represent the comfort level of passengers [45].

$$PMV = (0.303 * e^{-0.036M} + 0.028) * (M - \sum_{i=1}^6 f_i) \quad (16a)$$

$$f_1 = 3.05e^{-3} * (5733 - 6.99M - P_{cabin}rH_{cabin}) \quad (16b)$$

$$f_2 = 0, M < 58.15 \quad (16c)$$

$$f_3 = 1.7e^{-5}M(5867 - P_{cabin}rH_{cabin}) \quad (16d)$$

$$f_4 = 1.4e^{-3}M(34 - T_a) \quad (16e)$$

$$f_5 = 3.96e^{-8}f_{cl}[(T_{cl} + 273.15)^4 - (T_r + 273.15)^4] \quad (16f)$$

$$f_6 = f_{cl}\alpha_{cl}(T_{cl} - T_a) \quad (16g)$$

$$T_{cl} = 35.7 - 0.028M - R_{cl}(f_5 + f_6) \quad (16h)$$

where  $M$ , the metabolic rate of the passenger, is selected as 1 met;  $R_{cl}$ , clothes thermal resistance of the passenger is selected as 0.7 clo [46];  $T_{cl}$  is the surface temperature of the passenger's clothes, °C;  $T_r$  and  $T_{cabin}$  are the mean radiation temperature and cabin temperature, °C. For simplification,  $T_r$  can be set to be same as  $T_{cabin}$  [46]. The PMV value calculated using the aforementioned method represents the average comfort level of all passengers and the driver. The main control target in this study is the dry-bulb temperature obtained from the PMV calculator. The relative humidity is used as an input to the PMV calculator, as it has a minor impact on the PMV value [47].

The solution vector at time  $k$  can be written as  $u_{k+1}^* = \{u_{k+1|k}^*, \dots, u_{k+i|k}^*\}$ , where the first element was integrated into the TCCTMS at  $k + 1$ . A receding horizon control technique was developed to constantly improve the system by repeating the optimization problem at time  $k + 1$ .

The PMV value is regarded to be within the range of -0.5 to 0.5, indicating that the passengers are at a comfortable level. Among these, PMV=0 denotes the greatest level of comfort, while PMV=0.5 and PMV=-0.5 are regarded as the degrees of warmth or coldness that passengers experience. Two MPC strategies are used in this paper:

(1) Comfort priority MPC: The goal of PMV is set to 0 to ensure that passengers are in the most comfortable state;

(2) Energy saving priority MPC: reduce the cooling load as much as possible to save energy when ensuring passengers' comfort. The PMV objective is set at 0.47 to prevent small temperature variations in the vehicle as a result of abrupt speed changes.

## 4. Traditional controllers for TCCTMS

### 4.1 On/Off – PI Controller

Fig.7 shows the TCCTMS controlled by an On/Off-PI Controller. The system incorporates two On/Off controllers to regulate the  $N_{com}$  and the  $\dot{m}_{air}$  to maintain the

cabin temperature within a specific range. Additionally, a PI controller is employed to control the EEV to optimize the discharge pressure. In this study, the control objective of the  $P_{dis}$  is solely influenced by the ambient temperature, considering the impact of frequent starts and stops of the compressor on the PI controller. The control objective formula is derived from extensive simulations conducted to obtain reliable results.

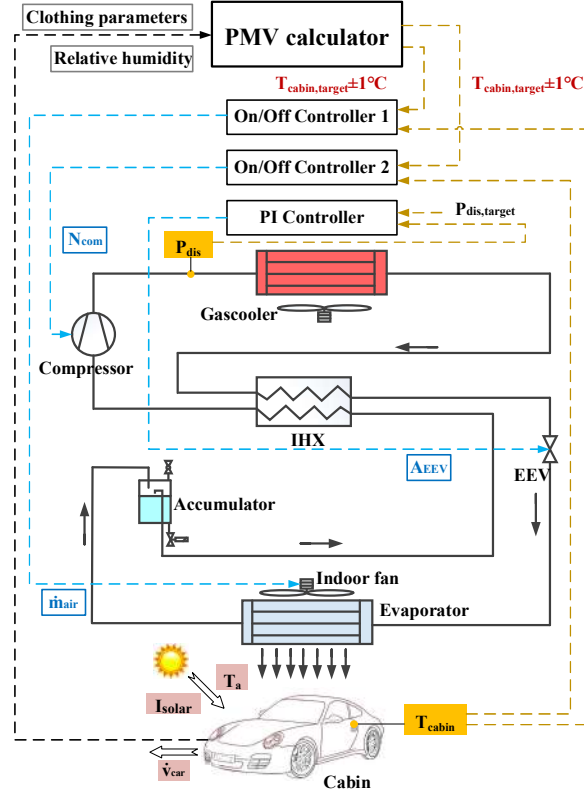


Fig.7 TCCTMS with On/Off-PI controller.

$$N_{com} = \begin{cases} 3500 & T_{cabin} > T_{cabin,target} + 1^\circ\text{C} \\ unchanged & T_{cabin,target} - 1^\circ\text{C} < T_{cabin} < T_{cabin,target} + 1^\circ\text{C} \\ 0 & T_{cabin} < T_{cabin,target} - 1^\circ\text{C} \end{cases} \quad (17)$$

$$\dot{m}_{air} = \begin{cases} 1.8 & T_{cabin} > T_{cabin,target} + 1^\circ\text{C} \\ unchanged & T_{cabin,target} - 1^\circ\text{C} < T_{cabin} < T_{cabin,target} + 1^\circ\text{C} \\ 0 & T_{cabin} < T_{cabin,target} - 1^\circ\text{C} \end{cases} \quad (18)$$

$$P_{dis,target} = 2.70 * T_a - 2.16 \quad (19)$$

## 4.2 PI Controller

Three PI controllers are intended to operate the TCCTMS, as depicted in Fig. 8. By adjusting  $\dot{m}_{air}$ , PI controller 1 brings  $T_{cabin}$  to the desired value. By changing

$N_{com}$ , PI controller 2 causes  $T_{send}$  to attain the goal value. The goal value is often set to 8 °C, as it is in this study, to guarantee that the cabin can be cooled to the desired temperature under all operational circumstances. By regulating  $A_{EEV}$ , PI controller 3 maintains the  $P_{dis}$  in the optimal range. The most important variables influencing the optimal discharge pressure are ambient temperature and outlet temperature of the gascooler, hence eq. 20 calculates  $P_{dis, target}$  in real-time. Eq. 20 was developed from several high-fidelity models' data fits.

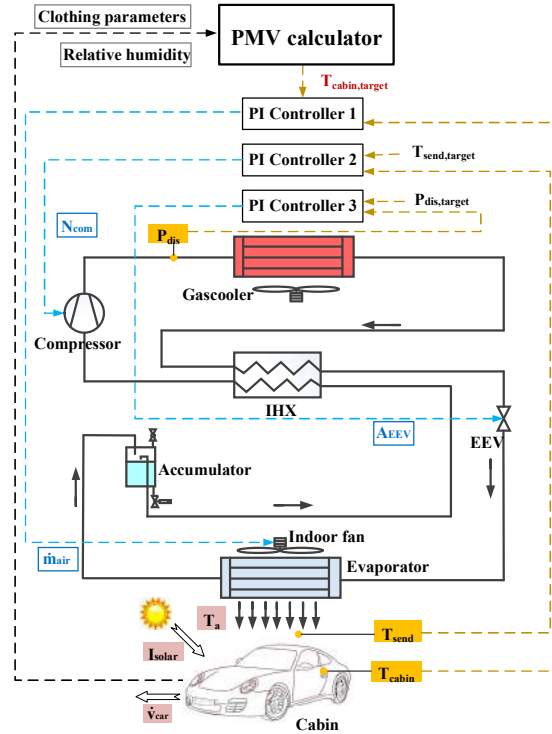


Fig.8 TCCTMS with PI controllers.

$$P_{dis,target} = -2.69 * T_a + 2.23 * T_{gc,out} - 7.13 \quad (20)$$

## 5. Study Case

In this section, we use the four control strategies mentioned in Section 4 to run the TCCTMS for 6 hours, from 9:00 to 15:00 on a certain summer day. The vehicle is operated according to the road conditions specified by the China Automotive Test Cycle (CLTC). Fig. 9 shows the changes in solar radiation intensity, ambient temperature and vehicle speed during the test.

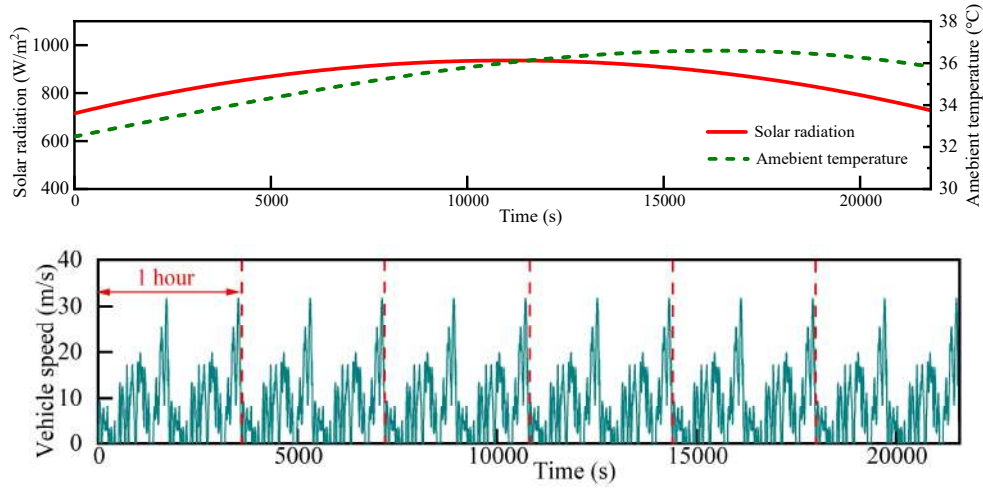


Fig.9 Trajectories of solar radiation, ambient temperature, and speed of the vehicle.

Fig. 10 illustrates the PMV values under the control of different strategies. The graph shows that the strategy using On/Off-PI controller causes fluctuations in the PMV range of -0.565 to 0.689 due to the hysteresis involved in the heating and cooling process. This fluctuation fails to ensure passenger comfort. Conversely, both the strategy using PI controller and the comfort priority MPC keep the PMV close to 0 during operation, with slight fluctuations influenced by the vehicle speed. However, the former may result in an overshoot of the cabin temperature during startup, temporarily reducing passenger comfort. In contrast, the comfort priority MPC successfully avoids this issue, ensuring a smoother and more comfortable experience for passengers. Furthermore, the energy saving priority MPC consistently maintains the PMV within the range of 0.385 to 0.499, ensuring continuous passenger comfort throughout the operation. Therefore, MPCs demonstrate advantages in ensuring passenger comfort.

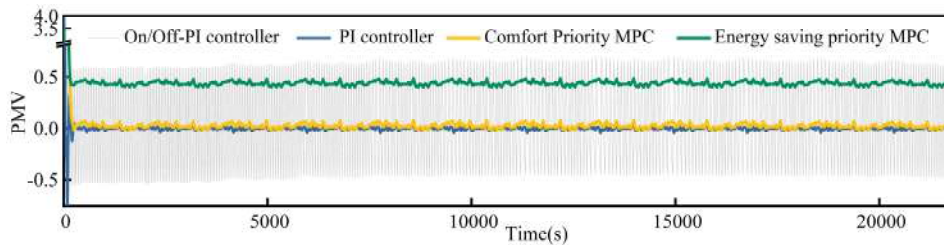
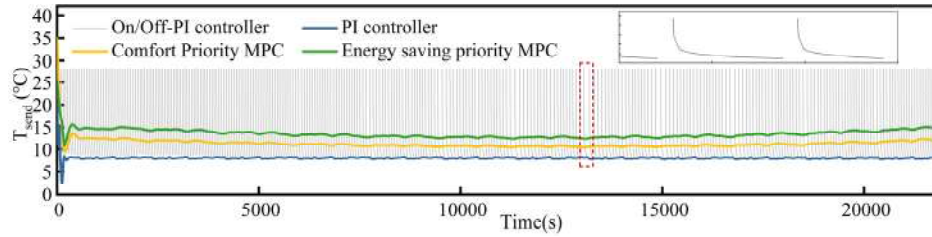


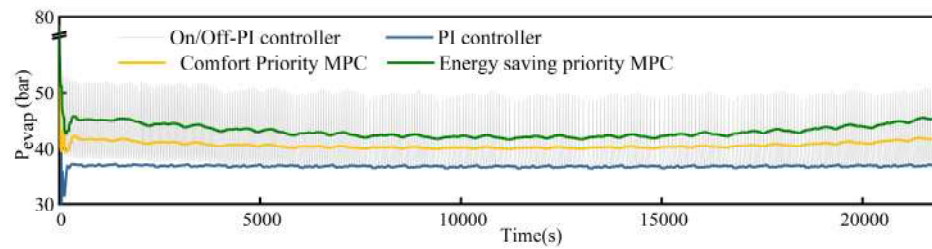
Fig.10 Trajectories of the PMV values under the control of On/Off-PI controller, PI controller, comfort priority MPC and energy saving priority MPC.

Fig. 11(a) shows the changes of the  $T_{\text{send}}$  values under the 4 control strategies. It can be seen that the strategies using MPC adjust  $T_{\text{send}}$  automatically based on the cabin's

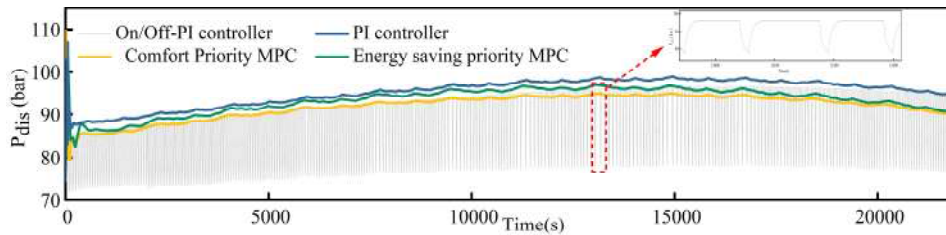
heat load, and the  $T_{\text{send}}$  values initially decrease and then rise. In addition, the  $T_{\text{send}}$  value with the energy-saving priority MPC (10.77 °C to 15.89 °C) is higher than that with the comfort priority MPC (9.26 °C to 13.80 °C). This results in the increase of the evaporation temperatures, as shown in Fig. 11(b). The comfort priority MPC keeps  $P_{\text{evap}}$  between 39.65 bar and 42.31 bar, while the energy-saving priority MPC maintains it between 41.41 bar and 45.83 bar. Besides, compared to the strategy using PI controller, both MPC strategies increase the maximum evaporation pressure by 5.02 bar (13.6%) and 8.67 bar (23.5%), respectively, contributing significantly to energy savings in the TCCTMS. In Fig. 11(c),  $P_{\text{dis}}$  controlled by the strategy using On/Off-PI controller, remains close to the optimal value determined by ambient temperature alone. However, the strategies using PI controller and MPC consider the influence of solar radiation, causing  $P_{\text{dis}}$  values to follow the cabin's heat load trend. The maximum values of  $P_{\text{dis}}$  occur at 13151s (when  $T_a$  is high and  $I_{\text{solar}}$  reaches its peak value) in all three strategies, measuring 98.75 bar, 95.03 bar, and 97.00 bar, respectively.



(a)



(b)

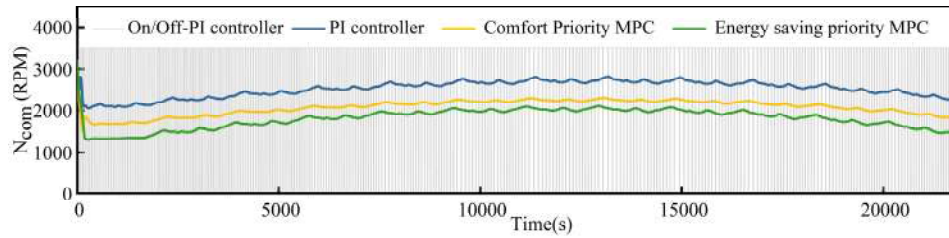


(c)

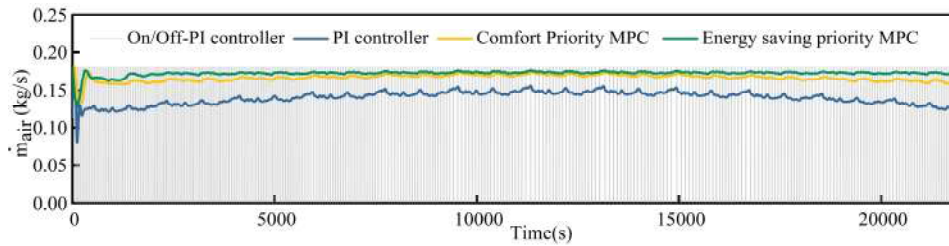
Fig.11 Trajectories of the (a)  $T_{\text{send}}$  (b)  $P_{\text{evap}}$  and (c)  $P_{\text{dis}}$  values under the control of On/Off -PI controller, PI controller, comfort priority MPC and energy saving

priority MPC.

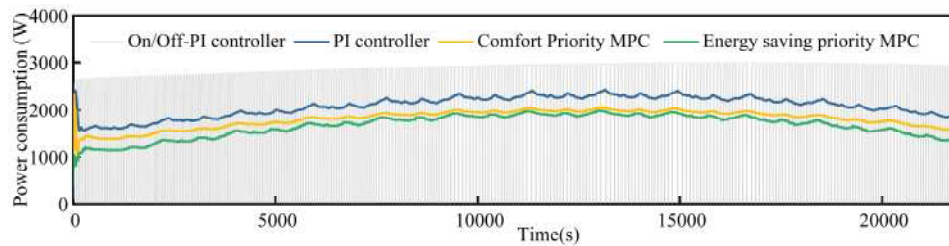
Fig. 12(a) and Fig. 12(b) indicate that the values of  $N_{com}$  and  $\dot{m}_{air}$  increase first and then decrease under the control of the PI controller and two MPCs. It can be observed that the compressor speed is higher under the PI control compared to the  $N_{com}$  under the two MPC controls. Notably, the energy-saving priority MPC control demonstrates the lowest compressor speed among the three control strategies. Conversely, the  $\dot{m}_{air}$  value under the PI control remains at the lowest. This can be attributed to the lower  $T_{send}$  and  $P_{evap}$  values with the PI controller compared to the two MPCs. In addition, as shown in Fig.12(c), the  $\dot{W}$  under the PI controller consistently surpasses that of the comfort priority MPC due to the low evaporation pressure and the heavy dehumidification load. Conversely, the energy-saving priority MPC exhibits the lowest power consumption. Overall, compared to the PI controller, both the comfort priority MPC and energy-saving priority MPC can achieve power consumption reductions of 7.89% to 17.58% and 15.17% to 29.99%, respectively.



(a)



(b)



(c)



Fig. 12 Trajectories of (a)  $N_{com}$ , (b)  $\dot{m}_{air}$ , (c)  $\dot{W}$  under the control of On/Off-PI controller, PI controller, Comfort priority MPC, and energy saving priority MPC.

Fig. 13 illustrates the energy consumption of the TCCTMS under the four controllers over a 6-hour period. It is evident that from 2500s to 17000s, the energy consumption of the On/Off-PI controller is lower than that of the PI controller. This is due to the On/Off-PI controller sacrificing some passenger comfort during periods of high cabin heat load. Furthermore, the comfort priority MPC demonstrates significant energy-saving advantages as it automatically determines the optimal  $T_{send}$  and  $P_{dis}$ . Compared to the On/Off-PI controller and PI controller, it achieves energy savings of 14.51% and 13.33%, respectively. In the case of energy-saving priority MPC, further optimization is achieved by increasing evaporation pressure and reducing heat load. This results in a total energy consumption reduction of 2.71 kWh/2.54 kWh (21.38%/20.27%) over the 6-hour period, compared to the On/Off-PI controller and PI controller.

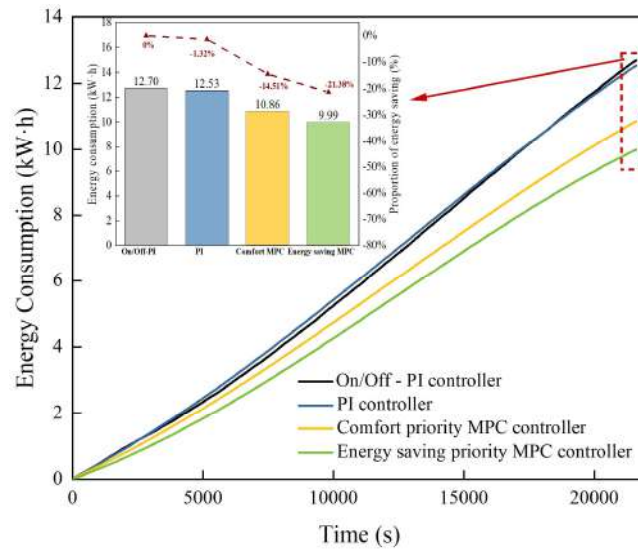


Fig. 13 Energy consumption trajectories of the TCCTMS under four controllers.

## 6. Conclusion

In this study, we provide a comfort priority model predictive controller and an energy saving priority model predictive controller for the transcritical  $CO_2$  system that focuses on the cabin cooling mode. Based on the genetic algorithm, an orienting control data-driven model is created for transcritical  $CO_2$  air conditioning system. Through

1 rigorous validation, we confirm the model's ability to accurately capture the dynamic  
2 behavior of the system. Besides, A dynamic cabin thermal model and a predicted mean  
3 vote calculator are established to predict and evaluate passenger comfort. In addition,  
4 comparisons are made between the proposed MPCs and traditional feedback control  
5 strategies, including On/Off-PI control and PI control, under various conditions such as  
6 variable ambient temperature, solar radiation, and vehicle speed over a 6-hour  
7 evaluation period. Key findings are reached and given as follows:

8 (1) The proposed model predictive controller enables simultaneous control of the  
9 compressor, expansion valve, and indoor fan under operating condition disturbances,  
10 without the need for an additional PI controller. This allows the transcritical CO<sub>2</sub> system  
11 to operate the optimal discharge pressure and optimal supply air temperature, without  
12 the need for extensive experimental selection of optimal values.

13 (2) The two model predictive controllers improve passenger comfort by maintaining  
14 stable PMV values, overcoming PMV fluctuations in On/Off-PI control, and  
15 eliminating PMV overshoot issues during startup in PI control.

16 (3) Both comfort priority model predictive controller and energy-saving priority model  
17 predictive controller exhibit notable reductions in power consumption compared to the  
18 PI controller. Comfort priority model predictive controller can achieve power savings  
19 of 7.89% to 17.58%, while energy-saving priority model predictive controller can  
20 achieve even greater power savings of 15.17% to 29.99%. Furthermore, the transcritical  
21 CO<sub>2</sub> cabin thermal management system equipped with two MPCs exhibits a significant  
22 reduction in total energy consumption, with a decrease of 13.33% (equivalent to 1.67  
23 kWh) and 20.27% (equivalent to 2.54 kWh) observed over a 6-hour duration.

24 This study represents an ongoing effort, with the current paper focusing solely on  
25 the cabin cooling mode. However, future research will encompass other aspects such  
26 as cabin heating, coordinated cooling and heating between the cabin and the battery, as  
27 well as cabin dehumidification. Exploring these areas could potentially lead to  
28 substantial modifications in the conclusions drawn from this study.

## 30 **Acknowledgment**

1 The corresponding author is grateful to the Foundation for Innovative Research Groups  
2 of the National Natural Science Foundation of China (No.51721004), the National  
3 Natural Science Foundations of China (No.52006161) and China Scholarship Council  
4 (No. 202206280214).  
5

## Reference

- [1] J. Cheng, S. Shuai, Z. Tang, T. changfa. Thermal performance of a lithium-ion battery thermal management system with vapor chamber and minichannel cold plate, *Applied Thermal Engineering*, 2023, 222, 119694.
- [2] The Kigali Amendment, The amendment to the montreal protocol agreed by the twenty-eighth meeting of the parties (Kigali, 10-15 October 2016), Ozone Secretariat, 2016.
- [3] Y. Song, H. Wang, Y. Ma, X. Yin, F. Cao, Energetic, economic, environmental investigation of carbon dioxide as the refrigeration alternative in new energy bus/railway vehicles' air conditioning systems, *Applied Energy*, 2022, 305(1), 117830.
- [4] D. Wang, B. Yu, J. Hu, L. Chen, J. Shi, J. Chen, Heating performance characteristics of CO<sub>2</sub> heat pump system for electrical vehicle in a cold climate, *International Journal of Refrigeration*, 2018, 85, 27-41.
- [5] H. Wang, Y. Song, Y. Qiao, S. Li, F. Cao, Rational assessment and selection of air source heat pump system operating with CO<sub>2</sub> and R407C for electric bus, *Renewable Energy*, 2022, 182, 86-101.
- [6] A. Okasha, N. Müller, K. Deb, Bi-objective optimization of transcritical CO<sub>2</sub> heat pump systems, *Energy*, 2022, 247(15), 123469.
- [7] Y. Song, C. Cui, X. Yin, F. Cao, Advanced development and application of transcritical CO<sub>2</sub> refrigeration and heat pump technology—A review, *Energy Reports*, 2022, 8, 7840-7869.
- [8] B. Yu, J. Yang, D. Wang, J. Shi, J. Chen, An updated review of recent advances on modified technologies in transcritical CO<sub>2</sub> refrigeration cycle, *Energy*, 2019, 189 (15), 116147.
- [9] Y. Yao, D. K. Shekhar, State of the art review on model predictive control (MPC) in Heating Ventilation and Air-conditioning (HVAC) field, *Building and Environment*, 2021, 200, 107952.
- [10] Y. Xie, Z. Liu, K. Li, J. Liu, Y. Zhang, D. Dan, C. Wu, P. Wang, X. Wang, An improved intelligent model predictive controller for cooling system of electric vehicle, *Applied Thermal Engineering*, 182 (2021) 116084.

- 1 [11] Y. Xie, J. Ou, W. Li, K. Li, J. Liu, Z. Liu, D. Zhou, J. Li, An intelligent eco-heating  
2 control strategy for heat-pump air conditioning system of electric vehicles, *Applied*  
3 *Thermal Engineering*, 2022, 216(5), 119126.
- 4 [12] J. Glos, L. Otava and P. Václavek, Non-Linear Model Predictive Control of Cabin  
5 Temperature and Air Quality in Fully Electric Vehicles, *IEEE Transactions on*  
6 *Vehicular Technology*, 2021, 70(2), 1216-1229.
- 7 [13] H. He, H. Jia, C. Sun, F. Sun, Stochastic Model Predictive Control of Air  
8 Conditioning System for Electric Vehicles: Sensitivity Study, Comparison, and  
9 Improvement, *IEEE Transactions on Industrial Informatics*, 2018, 14 (9), 4179-4189.
- 10 [14] S. Schaut, O. Sawodny, Thermal Management for the Cabin of a Battery Electric  
11 Vehicle Considering Passengers' Comfort, *IEEE Transactions on Control Systems*  
12 *Technology*, 2020, 28(4), 1476-1492.
- 13 [15] H. He, M. Yan, C. Sun, J. Peng, M. Li, H. Jia, Predictive air-conditioner control  
14 for electric buses with passenger amount variation forecast, *Applied Energy*, 2018, 227,  
15 249-261.
- 16 [16] M. Yan, H. Xu, L. Jin, H. He, M. Li, H. Liu, Co-optimization for fuel cell buses  
17 integrated with power system and air conditioning via multi-dimensional prediction of  
18 driving conditions, *Energy Conversion and Management*, 2022, 271(1), 116339.
- 19 [17] S. Hemmati, N. Doshi, D. Hanover, C. Morgan, M. Shahbakhti, Integrated cabin  
20 heating and powertrain thermal energy management for a connected hybrid electric  
21 vehicle, *Applied Energy*, 2021, 283(1), 116353.
- 22 [18] Y. Zhang, L. Tong, Regenerative braking-based hierarchical model predictive  
23 cabin thermal management for battery life extension of autonomous electric vehicles,  
24 *Journal of Energy Storage*, 2022, 52, Part A, 1, 104662.
- 25 [19] Y. Xie, C. Wang, X. Hu, X. Lin, Y. Zhang, W. Li, An MPC-Based Control Strategy  
26 for Electric Vehicle Battery Cooling Considering Energy Saving and Battery Lifespan,  
27 *IEEE Transactions on Vehicular Technology*, 2020, 69(12), 14657-14673.
- 28 [20] Y. Liu, J. Zhang, Self-adapting J-type air-based battery thermal management  
29 system via model predictive control, *Applied Energy*, 2020, 263(1), 114640.
- 30 [21] S. Park, C. Ahn, Computationally efficient stochastic model predictive controller

1 for battery thermal management of electric vehicle, IEEE Transactions on Vehicular  
2 Technology, 2020, 69(8), 1-13.

3 [22] M. R. Amini, H. Wang, X. Gong, D. Liao-McPherson, I. Kolmanovsky, J. Sun,  
4 Cabin and Battery Thermal Management of Connected and Automated HEVs for  
5 Improved Energy Efficiency Using Hierarchical Model Predictive Control, IEEE  
6 Transactions on Control Systems Technology, 2020, 28(5), 1711-1726.

7 [23] R. Guo, L. Li, Z. Sun, X. Xue, An integrated thermal management strategy for  
8 cabin and battery heating in range-extended electric vehicles under low-temperature  
9 conditions, Applied Thermal Engineering, 2023, 228 (25) , 120502.

10 [24] X. Gong, J. Wang, B. Ma, L. Lu, Y. Hu, H. Chen, Real-Time Integrated Power  
11 and Thermal Management of Connected HEVs Based on Hierarchical Model Predictive  
12 Control, IEEE/ASME Transactions on Mechatronics, 2021, 26, 3, 1271-1282.

13 [25] L. Guo, B. Ma, X. Gong, Y. Hu, H. Chen, Bilevel Predictive Control for HEVs  
14 Integrating Energy and Cabin Thermal Comfort, IEEE Transactions on Transportation  
15 Electrification, DOI 10.1109/TTE.2023.3274574.

16 [26] S.M. Liao, T.S. Zhao, A. Jakobsen, A correlation of optimal heat rejection  
17 pressures in transcritical carbon dioxide cycles, Applied Thermal Engineering, 20  
18 (2000) 831-841.

19 [27] J. Sarkar, S. Bhattacharyya, M.R. Gopal, Optimization of a transcritical CO<sub>2</sub> heat  
20 pump cycle for simultaneous cooling and heating applications, International Journal of  
21 Refrigeration, 27 (2004) 830-838.

22 [28] Y. Chen, J. Gu, The optimum high pressure for CO<sub>2</sub> transcritical refrigeration  
23 systems with internal heat exchangers, International Journal of Refrigeration, 28 (2005)  
24 1238-1249.

25 [29] S. Sawalha, Theoretical evaluation of trans-critical CO<sub>2</sub> systems in supermarket  
26 refrigeration. Part I: Modeling, simulation and optimization of two system solutions,  
27 International Journal of Refrigeration, 31 (2008) 516-524.

28 [30] C. Aprea, A. Maiorino, Heat rejection pressure optimization for a carbon dioxide  
29 split system: An experimental study, Applied Energy, 86 (2009) 2373-2380.

30 [31] P.-C. Qi, Y.-L. He, X.-L. Wang, X.-Z. Meng, Experimental investigation of the

1 optimal heat rejection pressure for a transcritical CO<sub>2</sub> heat pump water heater, *Applied*  
2 *Thermal Engineering*, 56 (2013) 120-125.

3 [32] S. Kim, J. Won, M. Kim, Effects of operating parameters on the performance of a  
4 CO<sub>2</sub> air conditioning system for vehicles, *Applied Thermal Engineering*, 2009, 29, 11–  
5 12, 2408-2416.

6 [33] Y. Chen, Optimal heat rejection pressure of CO<sub>2</sub> heat pump water heaters based  
7 on pinch point analysis, *International Journal of Refrigeration*, 2019, 106, 592-603.

8 [34] X. Qin, H. Liu, X. Meng, X. Wei, L. Zhao, L. Yang, A study on the compressor  
9 frequency and optimal heat rejection pressure of the transcritical CO<sub>2</sub> heat pump system,  
10 *International Journal of Refrigeration*, 2019, 99, 101-113.

11 [35] X. Yin, F. Cao, J. Wang, M. Li, X. Wang, Investigations on optimal heat rejection  
12 pressure in CO<sub>2</sub> heat pumps using the GMDH and PSO-BP type neural network—Part  
13 A: theoretical modeling, *International Journal of Refrigeration*, 2019, 106, 549-557.

14 [36] Y. Song, D. Yang, M. Li, F. Cao, Investigations on optimal heat rejection pressure  
15 in CO<sub>2</sub> heat pumps using the GMDH and PSO-BP type neural network—part B:  
16 experimental study, *International Journal of Refrigeration*, 2019, 106, 248-257.

17 [37] B. Hu, Y. Li, F. Cao, Z. Xing, Extremum seeking control of COP optimization for  
18 air-source transcritical CO<sub>2</sub> heat pump water heater system, *Applied Energy*, 2015, 147,  
19 361-372.

20 [38] C. Cui, J. Ren, M. Rampazzo, Y. Song, X. Yin, F. Cao, Real-time energy-efficient  
21 operation of a dedicated mechanical subcooling based transcritical CO<sub>2</sub> heat pump  
22 water heater via multi-input single-output extreme seeking control, *International*  
23 *Journal of Refrigeration*, 2022, 144, 76-89.

24 [39] C. Cui, J. Ren, Y. Song, X. Yin, W. Wang, X. Yang, F. Cao, Multi-variable  
25 extreme seeking control for efficient operation of sub-cooler vapor injection trans-  
26 critical CO<sub>2</sub> heat pump water heater, *Applied Thermal Engineering*, 2021, 184, 116261.

27 [40] M. Rampazzo, A. Cervato, C. Corazzol, L. Mattiello, A. Beghi, L. Cecchinato,  
28 Energy-efficient operation of transcritical and subcritical CO<sub>2</sub> inverse cycles via  
29 Extremum Seeking Control, *Journal of Process Control*, 2019, 81, 87-97.

30 [41] W. Wang, Z. Zhao, Q. Zhou, Y. Qiao, F. Cao, Model predictive control for the

- 1 operation of a transcritical CO<sub>2</sub> air source heat pump water heater, *Applied Energy*,  
2 2021, 300, 117339.
- 3 [42] T. Zhang, F. Cao, Y. Song, J. Ren, G. Bai, X. Pang, Y. He, The model predictive  
4 control strategy of the transcritical CO<sub>2</sub> air conditioning system used in railway vehicles,  
5 *Applied Thermal Engineering*, 2023, 218, 5, 119376.
- 6 [43] S.J. Kline, F.A. Mcclintock, Describing Uncertainties in Single-Sample  
7 Experiments, *Mechanical engineering*, 1953, 75, 3-9.
- 8 [44] A. Lambora, K. Gupta and K. Chopra, Genetic Algorithm- A Literature Review,  
9 2019 International Conference on Machine Learning, Big Data, Cloud and Parallel  
10 Computing (COMITCon), 2019, 380-384.
- 11 [45] P. O. Fanger, Thermal comfort. Analysis and applications in environmental  
12 engineering, *Thermal comfort. Analysis and applications in environmental engineering*,  
13 1970, 244.
- 14 [46] Y. Farzaneh, A.A. Tootoonchi, Controlling automobile thermal comfort using  
15 optimized fuzzy controller, *Applied Thermal Engineering*, 2008, 28 (14–15), 1906-  
16 1917.
- 17 [47] M. Simion, L. Socaciu, P. Unguresan, Factors which Influence the Thermal  
18 Comfort Inside of Vehicles, *Energy Procedia*, 2016, 85, 472-480.